
Training-free Composition of Pre-trained GFlowNets for Multi-Objective Generation

Seokwon Yoon¹ Youngbin Choi² Seunghyuk Cho² Seungbeom Lee² MoonJeong Park² Dongwoo Kim^{1,2}

Abstract

Generative Flow Networks (GFlowNets) learn to sample diverse candidates in proportion to a reward function, making them well-suited for scientific discovery, where exploring multiple promising solutions is crucial. Further extending GFlowNets to multi-objective settings has attracted growing interest since real-world applications often involve multiple, conflicting objectives. However, existing approaches require additional training for each set of objectives, limiting their applicability and incurring substantial computational overhead. We propose a training-free mixing policy that composes pre-trained GFlowNets at inference time, enabling rapid adaptation without finetuning or retraining. Importantly, our framework is flexible, capable of handling diverse reward combinations ranging from linear scalarization to complex non-linear logical operators, which are often handled separately in previous literature. We prove that our method exactly recovers the target distribution for linear scalarization and quantify the approximation quality for non-linear operators through a distortion factor. Experiments on a synthetic 2D grid and real-world molecule-generation tasks demonstrate that our approach achieves performance comparable to baselines that require additional training.

1. Introduction

Generative models for structured discrete objects, e.g., molecules (Jin et al., 2020; Guan et al., 2023; Huang et al., 2024; Qu et al., 2024), graphs (Liao et al., 2019; Jo et al., 2022; Martinkus et al., 2022; Jang et al., 2024; Zhou et al., 2024), and biological sequences (Ingraham et al., 2019; Truong Jr & Bepler, 2023; Koh et al., 2025), have become

¹Department of Computer Science & Engineering, POSTECH, South Korea ²Graduate School of Artificial Intelligence, POSTECH, South Korea. Correspondence to: Dongwoo Kim <dongwoo.kim@postech.ac.kr>.

essential tools for scientific discovery. Among these, Generative Flow Networks (GFlowNets) (Bengio et al., 2021; 2023; Jain et al., 2023a) have emerged as a particularly compelling framework for sampling diverse candidates from distributions proportional to a given reward function. Unlike traditional optimization methods (Sutton et al., 1998; Schulman et al., 2015; 2017) that converge to a single high-reward solution, GFlowNets generate samples with probabilities proportional to their rewards, enabling exploration of multiple promising candidates rather than concentrating on a single optimum.

While standard GFlowNets are trained with respect to a single reward function, many real-world scientific applications require balancing multiple, often conflicting objectives simultaneously (Nouhi et al., 2022; Harris et al., 2023; Lee et al., 2025; Ran et al., 2025). In practice, the optimal trade-off among these objectives is rarely known a priori, requiring practitioners to flexibly explore diverse compositions of objectives to identify candidates that best suit their downstream requirements. This has motivated recent efforts to extend GFlowNets to multi-objective settings through two primary strategies: scalarization and logical operations. Scalarization approaches aggregate multiple objectives into a single scalar reward via weighted sum to sample candidates across diverse trade-off profiles (Jain et al., 2023b; Zhu et al., 2023). Alternatively, logical operators, as exemplified by compositional sculpting (Garipov et al., 2023), combine distributions from separately trained models using logical operators such as the harmonic mean for conjunction or the contrast operator for subtraction. Specifically, this approach employs a classifier-guided framework to realize logical operations between base distributions via an auxiliary classifier.

Despite these approaches enabling multi-objective generation, they suffer from two critical limitations. First, both strategies require additional training, limiting their applicability to a predefined set of reward functions defined during the training phase. For instance, preference-conditioned GFlowNets (Jain et al., 2023b; Zhu et al., 2023) must be re-trained from scratch to incorporate new objectives, whereas compositional sculpting requires training a dedicated auxiliary classifier for each new set of objectives. Both ap-

proaches incur substantial overhead that often exceeds the cost of training the base GFlowNet (Garipov et al., 2023). Second, existing methods typically address only a single formulation of multi-objective combination, either scalarization or logical composition, lacking a unified framework for both. Consequently, developing a training-free methodology that directly composes pre-trained GFlowNets across arbitrary reward sets and diverse composition schemes remains a significant open challenge.

In this work, we present a training-free framework for composing pre-trained GFlowNets by mixing their policies at inference time. Our key insight is that the likelihood of visiting a state in each model provides natural weights for combining their generation processes. Intuitively, this prioritizes the model that considers the current state more relevant to its objective. We provide a theoretical analysis of our mixing rule for linear scalarization, which shows that the mixing policy exactly induces the target distribution in the linear scalarization scenario. For general composition operators, we analyze the total variation distance between the induced and target distributions, and empirically show that our mixing rule provides an accurate approximation in high-density regions where it matters most.

We conduct experiments on a synthetic 2D grid domain and real-world molecule generation tasks, including both fragment- and atom-based settings. On a synthetic 2D grid domain, our mixing policy achieves substantially lower error than preference-conditioned baselines for scalarization, maintaining stable performance even as the number of objectives increases. For logical operators, our method performs comparably to classifier-guided mixing while requiring no additional training. On molecular generation, our training-free approach matches or exceeds the sample quality of baselines that require retraining, and for logical operators, our method is significantly faster than classifier-guided composition during inference. Overall, experimental results demonstrate that our method enables diverse compositions without additional training while incurring minimal inference overhead.

2. Related Work

Multi-objective generation in GFlowNets. Multi-objective generation in GFlowNets has primarily been addressed through two strategies: scalarization and logical operators. Scalarization approaches transform multiple objectives into a single scalar reward through weighted combinations. Jain et al. (2023b) proposes MOGFN, which trains a single GFlowNet conditioned on preference vectors, enabling sampling across different trade-offs without retraining for each preference. Zhu et al. (2023) extends this idea with hypernetwork-based GFlowNets (HN-GFN) to improve sample efficiency, and Chen & Mauch (2024)

introduces order-preserving GFlowNets that learn from preference orderings without explicit reward scalarization. While these methods effectively explore the Pareto front, they require training a new model whenever a new objective is introduced, preventing the reuse of the existing model.

Logical operators offer an alternative by combining distributions learned by separately trained GFlowNets. Garipov et al. (2023) proposes compositional sculpting, which introduces logical operators such as harmonic mean for conjunction and contrast for subtraction. However, their method requires training an auxiliary classifier for each set of objectives, which often exceeds the cost of training the base GFlowNet itself.

Our work provides a unified training-free framework that covers both directions. By mixing pre-trained forward policies at inference time, we support scalarization across varying preference trade-offs and logical operators such as conjunction and subtraction, all without any additional training.

Model composition. Building complex distributions by composing pre-trained models has a rich history in machine learning. Products of experts (Hinton, 1999; 2002) combine multiple probabilistic models by multiplying their densities. In energy-based models, composition enables constructing complex concepts through algebraic operations on energy functions (Du et al., 2020; 2021). Recent work extends these ideas to diffusion models, enabling compositional generation through score function combination (Liu et al., 2022; Du et al., 2023). In diffusion models, classifier guidance (Dhariwal & Nichol, 2021; Ho & Salimans, 2021) provides post-hoc control by steering generation toward desired attributes without retraining. Beyond probability-space operations, weight-space averaging provides an alternative approach: model soups (Wortsman et al., 2022) and rewarded soups (Ramé et al., 2023) combine fine-tuned models by interpolating their parameters. For GFlowNets, compositional sculpting (Garipov et al., 2023) represents the first attempt at model composition, but requires training a classifier for each new composition. Our work proposes training-free model composition for multi-objective generation.

3. Background

In this section, we review the foundations of GFlowNets, including the reaching probability. We also describe the multi-objective generation problem.

3.1. Generative Flow Networks (GFlowNets)

GFlowNets (Bengio et al., 2021; 2023) are generative models designed to sample structured objects x , such as graphs or molecules, from a discrete space \mathcal{X} . The primary goal is to sample objects from a distribution $p(x)$ proportional to a

given non-negative reward function $R(x)$:

$$p(x) = \frac{R(x)}{Z}, \quad \text{where } Z = \sum_{x \in \mathcal{X}} R(x).$$

In practice, a temperature parameter β is often used to control the sharpness of the distribution, yielding $p(x) \propto R(x)^\beta$. Increasing β concentrates probability mass on high-reward candidates (Bengio et al., 2021).

To sample from such a distribution, GFlowNets model the generation as a sequential construction process governed by a stochastic forward policy p_F . Starting from an initial state s_0 , the policy samples an action to transition to a new state, progressively building up the object until reaching a terminating state $x \in \mathcal{X}$ and transitioning to the sink state s_f , which marks the completion of a trajectory. Formally, this process is defined over a directed acyclic graph (DAG) $(\mathcal{S}, \mathcal{A})$, where \mathcal{S} is a set of states and $\mathcal{A} \subseteq \mathcal{S} \times \mathcal{S}$ is a set of directed edges representing actions. There exist two distinguished states: a unique initial state $s_0 \in \mathcal{S}$ where all trajectories begin, and a unique sink state $s_f \in \mathcal{S}$ where all trajectories terminate. The set of terminating states $\mathcal{X} \subset \mathcal{S}$ consists of states that can transition to s_f via a terminating edge, though they may also transition to other states in \mathcal{S} . The forward policy p_F defines a distribution $p_F(\cdot|s)$ over the children of state $s \in \mathcal{S} \setminus \{s_f\}$, inducing a distribution over complete trajectories $\tau = (s_0 \rightarrow s_1 \rightarrow \dots \rightarrow s_n = x \rightarrow s_f)$, where $x \in \mathcal{X}$ represents the constructed object.

Reaching probability. A key quantity that will play a central role in our method is the reaching probability $u(s)$, defined as the probability of visiting state s when starting from s_0 under the forward policy p_F (Bengio et al., 2023):

$$u(s) := \sum_{\tau \in \mathcal{T}_{s_0, s}} \prod_{t=1}^T p_F(s_t | s_{t-1}), \quad (1)$$

where $\mathcal{T}_{s_0, s}$ denotes the set of all trajectories from s_0 to s . By definition, $u(s_0) = 1$ since every trajectory begins at s_0 . Intuitively, $u(s)$ captures how much probability mass the policy routes through state s , and satisfies the recursion:

$$u(s) = \sum_{s_*: (s_* \rightarrow s) \in \mathcal{A}} u(s_*) p_F(s | s_*). \quad (2)$$

For a terminating state $x \in \mathcal{X}$, the terminating state probability decomposes as:

$$p(x) = u(x) \cdot p_F(s_f | x). \quad (3)$$

This factorization separates the probability of reaching x from the probability of stopping at x .

3.2. Multi-Objective Generation in GFlowNets

Prior work in GFlowNets has addressed the multi-objective generation problem by enabling a single model to cover a family of compositions over multiple reward functions $\mathbf{R}(x) = (R_1(x), \dots, R_k(x))$. Jain et al. (2023b); Zhu et al. (2023) focus on scalarization, where multiple objectives are combined via a weighted sum, scaled by temperature β : $\tilde{R}(x) = (\sum_{i=1}^k \omega_i R_i(x))^\beta$. By conditioning the policy on the preference vector $\omega := (\omega_1, \dots, \omega_k)$, a single model learns to sample from distributions corresponding to arbitrary weight combinations within a fixed set of reward functions.

Compositional sculpting (Garipov et al., 2023) takes a different approach: given separately trained GFlowNets for each reward function, it enables sampling from distributions defined by logical operators (e.g., conjunction, subtraction) over the component distributions through training an auxiliary model. Specifically, it introduces two logical operators. The harmonic mean operator (\otimes) acts as a conjunction, assigning high probability only where all component distributions have high density: $(p_1 \otimes p_2)(x) \propto \frac{p_1(x)p_2(x)}{p_1(x)+p_2(x)}$. The contrast operator (\bullet) functions as a subtraction, highlighting regions where the first distribution dominates: $(p_1 \bullet p_2)(x) \propto \frac{p_1(x)^2}{p_1(x)+p_2(x)}$. These binary operators can be extended to more than two distributions through chaining. For a detailed discussion on the generalization of these operators, please refer to Garipov et al. (2023).

Following the setting of compositional sculpting, we assume access to a set of pre-trained GFlowNets $\{p_{i,F}\}_{i=1}^k$, where each $p_{i,F}$ is trained to sample from a distribution proportional to its corresponding reward function $R_i(x)$.

4. Method

In this section, we propose a training-free framework that composes pre-trained GFlowNets by mixing their forward policies at inference time (Section 4.1). We prove its exactness for linear scalarization and analyze the approximation error for non-linear operators (Section 4.2).

4.1. Mixture of GFlowNets

As described in Section 3.2, we assume access to k pre-trained GFlowNets, where each i -th GFlowNet is trained on reward function $R_i(x)$ and induces a terminating state distribution $p_i(x) \approx p_i^*(x) = R_i(x)/Z_i$. Our goal is to sample from a target distribution $p_M^*(x) \propto \mathcal{G}(p_1(x), \dots, p_k(x))$, where \mathcal{G} specifies how the component distributions are combined. Crucially, we aim to achieve this using only the pre-trained forward policies at inference time, without any additional training.

For the i -th component GFlowNet, we denote its forward

policy by $p_{i,F}$, reaching probability by u_i , and terminating state distribution by p_i . We define the mixing policy as:

$$p_{M,F}(s'|s) = \frac{\mathcal{G}(u_1(s)p_{1,F}(s'|s), \dots, u_k(s)p_{k,F}(s'|s))}{N_M(s)}, \quad (4)$$

where the local normalization constant $N_M(s)$ is

$$\sum_{s':(s \rightarrow s') \in \mathcal{A}} \mathcal{G}(u_1(s)p_{1,F}(s'|s), \dots, u_k(s)p_{k,F}(s'|s)). \quad (5)$$

The mixing policy weights each model’s transition probability $p_{i,F}(s'|s)$ by its reaching probability $u_i(s)$, then combines them through the composition function \mathcal{G} .

Reaching probability estimation. Computing $u_i(s)$ via the recursion Eq. (2) requires summing over all parent states, which is intractable in large state spaces. Instead, we utilize the different definition of the reaching probability which is expressed as $u_i(s) = F_i(s)/Z_i$, where $F_i(s)$ is the state flow and Z_i is the total flow (see Appendix A.2 for derivation). Since GFlowNet training objectives such as flow matching, detailed balance (Bengio et al., 2021), and sub-trajectory balance (Madan et al., 2023) jointly learn $F_i(s)$ and Z_i , we can directly leverage these learned quantities to compute $u_i(s)$.

4.2. Analysis of the Induced Distribution

To understand when our mixing policy recovers the target distribution, we first derive its general form. The distribution induced by our mixing policy takes the form:

$$\begin{aligned} p_M(x) &= u_M(x) \cdot p_{M,F}(s_f | x) \\ &= \frac{u_M(x)}{N_M(x)} \cdot \mathcal{G}(p_1(x), \dots, p_k(x)), \end{aligned} \quad (6)$$

where the *distortion factor* $\delta(x) := u_M(x)/N_M(x)$ measures how much the induced distribution deviates from the target. When $\delta(x)$ is constant across all x , our mixing policy exactly recovers the target distribution $p_M^*(x) \propto \mathcal{G}(p_1(x), \dots, p_k(x))$. We examine linear scalarization, where exact recovery is guaranteed, and non-linear operators, where approximations may arise.

Linear scalarization. Linear scalarization combines multiple objectives via a weighted sum. Given a preference vector $\omega = (\omega_1, \dots, \omega_k)$ with $\omega_i \geq 0$, the target distribution is:

$$p_M^*(x) \propto \sum_{i=1}^k \omega_i R_i(x). \quad (7)$$

The corresponding composition function is $\mathcal{G}(p_1, \dots, p_k) = \sum_{i=1}^k \omega_i Z_i p_i$. For this setting, $\delta(x)$ becomes constant, yielding exact recovery:

Proposition 4.1 (Exact realization for linear scalarization). *Given k GFlowNets with terminating distributions $p_i(x) \propto R_i(x)$, the mixing policy Eq. (4) under linear scalarization exactly realizes the target distribution:*

$$p_M(x) = p_M^*(x) \propto \sum_{i=1}^k \omega_i R_i(x), \quad (8)$$

where p_M is the distribution induced by our mixing policy.

The proof is provided in Appendix A.1. This is, to our knowledge, the first training-free method with provable exactness guarantees for the composition of multi-objective GFlowNets.

Non-linear composition operators. For non-linear composition operators, including scalarization with $\beta \neq 1$ where $\mathcal{G}(p_1, \dots, p_k) = (\sum_{i=1}^k \omega_i Z_i p_i)^\beta$, and the logical operators introduced in Section 3.2, $\delta(x)$ is not guaranteed to be constant, potentially introducing deviations from the target distribution. We empirically analyze in Section 5.3 that $\delta(x)$ remains approximately constant in high-reward regions most relevant to sampling, suggesting that our mixing policy provides accurate approximations where it matters most.

5. Synthetic Experiments

We conduct synthetic experiments on a 2D grid domain to validate our framework under controlled conditions where ground-truth distributions are computable.

5.1. Experimental Settings

Tasks. We use a 32×32 2D grid domain (Bengio et al., 2021), where the policy learns to navigate from the start state to high-reward regions. In this setting, each state corresponds to a grid cell, and the start state is the upper-left cell $s_0 = (0, 0)$. At each state, the policy takes one of three actions: move right, move down, or terminate at the current state. We utilize five standard benchmark rewards and three synthetic circle rewards, all defined over the grid cells and normalized to the range $[0, 1]$ (Fig. A1).

We conduct experiments on both scalarization and logical operators. For scalarization, we select subsets of size 2 to 5 from the five base rewards, use 128 evenly spaced preference vectors ω on the simplex for each subset, and evaluate the mixing policy under each preference. For logical operators, we evaluate various combinations of harmonic mean and contrast operations applied to the base and circle rewards.

Baselines. We evaluate our method on both scalarization and logical operators, comparing against baselines that require additional training. For scalarization, we consider preference-conditioned GFlowNets, including

Table 1. L_1 error on scalarization in a 2D grid with varying number of objectives. N Obj. denotes scalarization with N objectives, where the specific objectives used are detailed in Table A1. Results are averaged over 128 evenly spaced preference vectors.

	2 Obj.	3 Obj.	4 Obj.	5 Obj.
MOGFN	0.021	0.027	0.042	0.048
HN-GFN	0.017	0.021	0.032	0.035
Ensemble	0.117	0.098	0.113	0.111
Ours	0.003	0.003	0.003	0.003

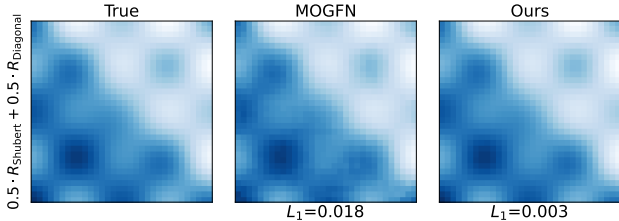


Figure 1. Qualitative result of scalarization on a 2D grid domain. We visualize the density on each grid of the true distribution (left), MOGFN (middle), and ours (right).

MOGFN (Jain et al., 2023b) and HN-GFN (Zhu et al., 2023). For logical operators, we compare against the classifier guidance approach of Garipov et al. (2023). For both settings, we also include a simple ensemble baseline that mixes forward policies without the reaching probability $u_i(\cdot)$ to validate the importance of flow-based weighting.

Evaluation metrics. In this setting, where the true target distribution and induced target distribution can be computed exactly, we evaluate the approximation quality using the L_1 error, i.e., $\sum_x |p_{\text{model}}(x) - p_{\text{target}}(x)|$, between the distribution induced by our mixing policy and the ground-truth target distribution, following Bengio et al. (2021).

We set $\beta = 1$ in this task. Further details on experimental settings and additional results are provided in Appendix B.1.

5.2. Results

Scalarization. Table 1 presents the average L_1 error over 128 evenly spaced preference vectors for varying numbers of objectives. Our mixing policy consistently outperforms the baselines across all settings. Notably, as the number of objectives increases from 2 to 5, our method maintains nearly constant error, whereas MOGFN and HN-GFN degrade with more objectives. The simple ensemble exhibits substantially higher L_1 error than ours, demonstrating that naive mixing without reaching probability weighting fails to approximate the target distribution.

For the two-objective setting, we additionally train single-objective GFlowNets separately for each of five fixed preference vectors. As shown in Fig. A2, our mixing policy outperforms even these individually trained models. Fig. 1 shows

Table 2. L_1 error on logical operators in a 2D grid. We evaluate harmonic mean (\otimes) and contrast (\odot) operations across different reward pairs. Additional results are provided in Table A2.

	Classifier guidance	Ensemble	Ours
<i>Harmonic mean (\otimes)</i>			
$p_{\text{Shubert}} \otimes p_{\text{Sphere}}$	0.158	0.145	0.136
$p_{\text{Shubert}} \otimes p_{\text{Diagonal}}$	0.142	0.190	0.180
$p_{\text{Circle1}} \otimes p_{\text{Circle2}}$	0.397	0.453	0.229
<i>Contrast (\odot)</i>			
$p_{\text{Shubert}} \odot p_{\text{Sphere}}$	0.175	0.175	0.111
$p_{\text{Sphere}} \odot p_{\text{Shubert}}$	0.190	0.162	0.116
$p_{\text{Shubert}} \odot p_{\text{Diagonal}}$	0.150	0.190	0.106
$p_{\text{Diagonal}} \odot p_{\text{Shubert}}$	0.153	0.190	0.158
$p_{\text{Circle1}} \odot p_{\text{Circle2}}$	0.245	0.356	0.231
$p_{\text{Circle2}} \odot p_{\text{Circle1}}$	0.241	0.390	0.070

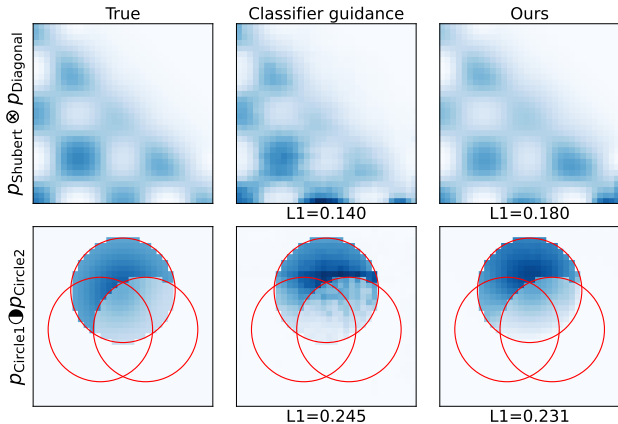


Figure 2. Qualitative result of logical operations on a 2D grid domain. We visualize the density on each grid of the true distribution (left), classifier guidance (middle), and ours (right).

the qualitative results. Our mixing policy more accurately recovers the multi-modal structure of the true distribution, whereas MOGFN produces slightly blurred modes.

Logical operators. Table 2 compares the ground-truth composition distributions with those induced by our mixing rule and baselines. Our mixing policy achieves comparable performance to the classifier-guided approach, with results varying across different composition types: our method outperforms on some compositions while the classifier-guided baseline performs better on others. Notably, our method achieves this competitive performance without requiring any additional training, whereas the classifier-guided approach requires training an auxiliary classifier for each new composition. Furthermore, our mixing policy consistently outperforms the simple ensemble baseline, demonstrating that the reaching probability weighting $u_i(\cdot)$ is essential for approximating target distributions under logical operators, not just scalarization.

Fig. 2 shows qualitative results of classifier-guided and our

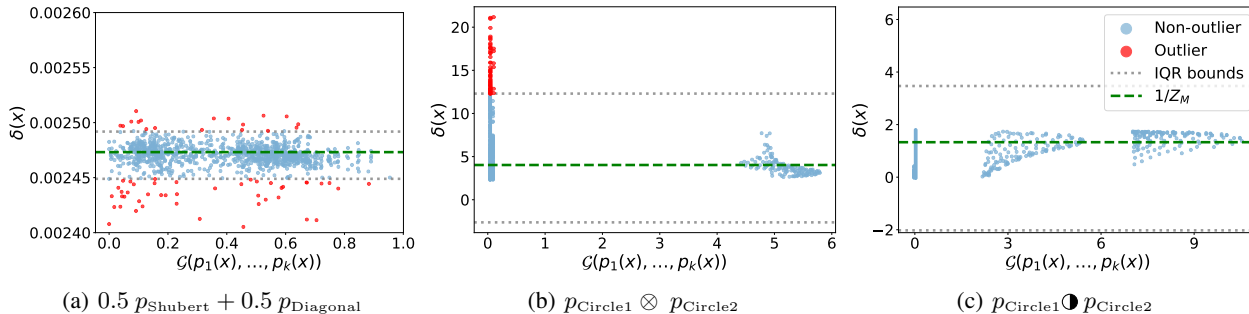


Figure 3. Distortion factor $\delta(x) = u_M(x)/N_M(x)$ vs. unnormalized target density $\mathcal{G}(p_1(x), p_2(x))$ on the 2D grid domain. Red points indicate outliers, defined as states where $\delta(x)$ falls outside $[Q_1 - 1.5 \cdot \text{IQR}, Q_3 + 1.5 \cdot \text{IQR}]$ (gray dotted lines), where Q_1, Q_3 are the 25th/75th percentiles and $\text{IQR} = Q_3 - Q_1$. The green dashed line marks $1/Z_M$ with $Z_M = \sum_x \mathcal{G}(p_1(x), p_2(x))$. Additional results are in Fig. A6.

mixing policy. Both successfully achieve the intended behavior of each operator: concentrating probability mass on regions where both component distributions have high density for the harmonic mean, and isolating regions where only the first distribution dominates for contrast.

5.3. Analysis of Approximation Quality

As discussed in Section 4.2, for non-linear composition operators, the distortion factor $\delta(x)$ is not guaranteed to be constant, potentially introducing deviations from the target distribution. Here, we empirically analyze how $\delta(x)$ behaves in practice.

To quantify the approximation error, we consider the L_1 distance between the induced distribution $p_M(x)$ and the target distribution $p_M^*(x)$:

$$\begin{aligned} L_1 &= \sum_x |p_M(x) - p_M^*(x)| \\ &= \sum_x \left| \delta(x) - \frac{1}{Z_M} \right| \mathcal{G}(p_1(x), \dots, p_k(x)), \quad (9) \end{aligned}$$

where $Z_M = \sum_x \mathcal{G}(p_1(x), \dots, p_k(x))$. We provide the detailed derivation in Appendix A.3. To analyze the approximation quality, we compute $1/Z_M$, the distortion factor $\delta(x)$ and the composition value $\mathcal{G}(p_1(x), \dots, p_k(x))$ for each x .

Fig. 3 visualizes how $\delta(x)$ varies with $\mathcal{G}(p_1(x), p_2(x))$ across different composition operators. For linear scalarization, Fig. 3(a) confirms that $\delta(x)$ remains constant at $1/Z_M$ across all samples, as expected from Proposition 4.1. For logical operators, Figs. 3(b) and 3(c) show that $\delta(x)$ is not exactly constant but remains close to $1/Z_M$ in high-composition value regions where $\mathcal{G}(\cdot)$ is large. Deviations primarily occur in low-composition value regions where $\mathcal{G}(\cdot)$ is small, contributing minimally to the overall L_1 error. This confirms that our mixing policy provides accurate approximations for samples that contribute most to the target distribution. Additional results are provided in Fig. A6.

6. Real-world Experiments

We evaluate our framework on real-world molecular generation tasks to demonstrate its practical applicability.

6.1. Experimental Settings

Tasks. We evaluate our framework on two tasks: fragment- and atom-based molecule generation. In fragment-based generation, molecules are assembled from a pre-defined vocabulary of 72 fragments. At each step, the policy selects a fragment and specifies attachment points on both the existing structure and the new fragment, with a maximum limit of 9 fragments per molecule. We employ three reward functions: (i) SEH, which measures the predicted binding affinity to soluble epoxide hydrolase using a pre-trained proxy model (Bengio et al., 2021); (ii) SA, which estimates synthetic accessibility (Ertl & Schuffenhauer, 2009); and (iii) QED, which quantifies drug-likeness (Bickerton et al., 2012). All rewards are normalized to $[0, 1]$ with larger values indicating better molecules.

For atom-based generation (QM9), molecules are constructed atom-by-atom and bond-by-bond. In this setting, each state is represented as a connected graph, and actions consist of adding a new node with an associated edge or modifying the attributes of an existing edge. We consider three reward functions: GAP, defined as the HOMO-LUMO gap predicted by an MXMNet (Zhang et al., 2020) proxy trained on the QM9 dataset (clipped to $[0, 2]$); and the aforementioned SA and QED.

As in the synthetic experiments, we evaluate both scalarization and logical operators. For scalarization, we use 10 and 128 evenly spaced preference vectors for two- and three-objective settings, respectively. For logical operators, we test various combinations applied to the base rewards.

Evaluation metrics. Unlike the grid experiments, neither the target nor the induced distributions can be computed

Table 3. Results of scalarization on molecule generation tasks. We report the average reward and diversity of the top-10 samples across different objective pairs. *ALL* denotes scalarization with all the three objectives.

		Reward			Diversity		
		MOGFN	HN-GFN	Ours	MOGFN	HN-GFN	Ours
Fragment	SEH-SA	0.839	0.885	0.836	0.572	0.603	0.556
	SEH-QED	0.759	0.772	0.773	0.562	0.595	0.565
	SA-QED	0.779	0.876	0.793	0.623	0.658	0.621
	ALL	0.793	0.747	0.790	0.663	0.659	0.643
QM9	GAP-SA	0.816	0.805	0.876	0.908	0.904	0.889
	GAP-QED	0.787	0.788	0.780	0.865	0.843	0.873
	SA-QED	0.648	0.531	0.729	0.901	0.916	0.722
	ALL	0.727	0.625	0.734	0.904	0.899	0.857

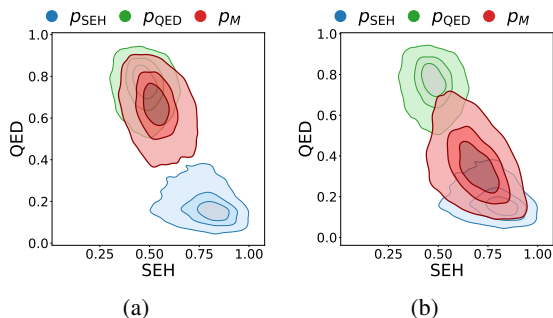


Figure 4. Density visualization of p_{SEH} , p_{QED} , and the composed distribution p_M induced by our mixing policy via scalarization on fragment-based molecule generation. Each distribution is estimated from 5,000 samples. We vary the weights as (a) $p_M \propto (0.3 \cdot R_{SEH} + 0.7 \cdot R_{QED})^{32}$ and (b) $p_M \propto (0.7 \cdot R_{SEH} + 0.3 \cdot R_{QED})^{32}$.

due to the large state space. For scalarization, we evaluate sample quality using the mean reward of top-10 samples and diversity ($1 - \text{Tanimoto similarity}$) among 128 generated samples (Jain et al., 2023b). For logical composition, following Garipov et al. (2023), we categorize 5,000 samples into $2^3 = 8$ bins based on whether each reward is above or below a threshold and report the percentage in each bin.

We use the same baselines as in the synthetic experiments, excluding the simple ensemble baseline. For the temperature parameter, we set $\beta = 32$ except for scalarization in fragment-based generation, where we use $\beta = 64$. Further details are provided in Appendix B.2.

6.2. Results

Scalarization. Table 3 presents the scalarization results for both fragment-based and atom-based molecule generation. In fragment-based generation, HN-GFN achieves the highest rewards on SEH-SA and SA-QED, while our method performs comparably to MOGFN. In QM9, our method achieves the highest average rewards on GAP-SA, SA-QED, and the three-objective setting, while baselines exhibit better diversity. Overall, neither method consistently outperforms the other, demonstrating that our training-free approach matches the performance of preference-

Table 4. Results of logical operators on molecule generation tasks. We report the percentage of 5,000 samples falling into the *target bin*: for harmonic mean (\otimes), where all composed objectives are high; for contrast (\ominus), where only the first objective is high.

	Fragment-based		Atom-based (QM9)	
	Classifier guidance	Ours	Classifier guidance	Ours
<i>Harmonic mean (\otimes)</i>				
$p_{SEH} \otimes p_{SA}$	78	92	$p_{GAP} \otimes p_{SA}$	57
$p_{SEH} \otimes p_{QED}$	78	92	$p_{GAP} \otimes p_{QED}$	61
$p_{SA} \otimes p_{QED}$	85	93	$p_{SA} \otimes p_{QED}$	72
$p_{SEH} \otimes p_{SA} \otimes p_{QED}$	42	74	$p_{GAP} \otimes p_{SA} \otimes p_{QED}$	21
<i>Contrast (\ominus)</i>				
$p_{SEH} \ominus p_{SA} \ominus p_{QED}$	60	67	$p_{GAP} \ominus p_{SA}$	85
$p_{SA} \ominus p_{SEH} \ominus p_{QED}$	74	83	$p_{GAP} \ominus p_{QED}$	86
$p_{QED} \ominus p_{SEH} \ominus p_{SA}$	38	45	$p_{GAP} \ominus p_{SA} \ominus p_{QED}$	74

conditioned models that require additional training. Fig. 4 shows scalarization with different preference vectors ω . As ω shifts toward one objective, the induced distribution moves toward the corresponding high-reward region.

Logical operators. Table 4 reports the percentage of samples in the target bin for each composition of the models. For the harmonic mean, the target bin is where all composed objectives are high; for the contrast operator, it is where only the first objective is high and the remaining objectives are low. Our method consistently achieves high target bin percentages, outperforming the classifier guidance.

Table A3 presents the detailed distribution of samples across all reward bins for the base GFlowNets and their compositions with our mixing policy. In single-objective models, samples concentrate on high values of their respective training rewards, with variation across the other rewards. For the harmonic mean operator, our mixing policy successfully concentrates samples on molecules scoring high in all composed objectives, and extending to three objectives further amplifies this effect. For the contrast operator, our mixing policy effectively emphasizes the first objective while suppressing the others, isolating regions distinctive to the first component. These results confirm that our training-free mixing policy correctly induces the intended compositional behaviors across both operators.

Fig. 5 visualizes the reward distributions induced by the classifier-guided and our mixing policy. Figs. 5(a) and 5(b) show the results on the harmonic mean of SEH and SA ($p_{SEH} \otimes p_{SA}$). Our mixing policy produces samples concentrated in regions where both rewards are high, whereas the classifier-guided mixing policy often produces high-SA but low-SEH samples. Figs. 5(c) and 5(d) present the results on the contrast of SA and SEH ($p_{SA} \ominus p_{SEH}$). Our mixing policy successfully isolates samples scoring high only on SA while suppressing the high-SEH region, as intended by the contrast operator. Conversely, the classifier guidance produces a distribution that nearly coincides with the base SA distribution (p_{SA}), failing to achieve the subtraction effect.

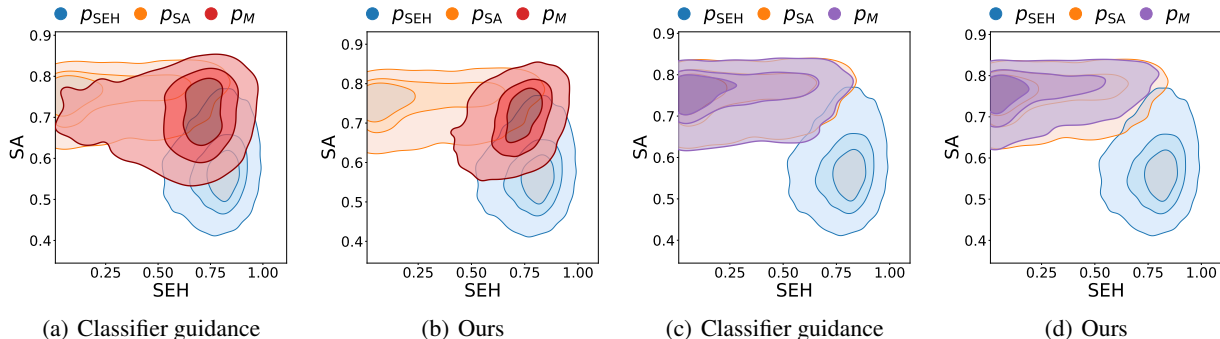


Figure 5. Distributions p_M induced by classifier-guided and our mixing policy for fragment-based molecule generation. Each distribution is estimated from 5,000 samples. Base distributions p_{SEH} and p_{SA} are shown alongside the composed distribution. (a) Classifier-guided mixing policy on $p_{SEH} \otimes p_{SA}$. (b) Ours on $p_{SEH} \otimes p_{SA}$. (c) Classifier-guided mixing policy on $p_{SA} \odot p_{SEH}$. (d) Ours on $p_{SA} \odot p_{SEH}$.

Table 5. Inference cost comparison on molecule generation tasks. We report the average generation time (ms) and trajectory length over 1,000 samples. We use preference vectors $\omega \in \{(0.5, 0.5), (0.33, 0.33, 0.34)\}$ for scalarization, and the harmonic mean for compositional operators.

	#Obj.	Fragment-based		Atom-based (QM9)		
		Time (ms)	Traj. Len.	Time (ms)	Traj. Len.	
Scalarization	2	MOGFN	16.05	26.0	12.71	15.2
		HN-GFN	15.84	25.8	17.44	19.0
		Ours	23.56	25.9	41.79	30.1
Scalarization	3	MOGFN	15.75	26.0	24.14	27.9
		HN-GFN	15.30	26.0	32.69	36.8
		Ours	27.28	25.5	46.39	29.6
Composition	2	Classifier guidance	1789.11	25.9	1494.22	31.6
		Ours	24.70	25.9	37.64	29.2
	3	Classifier guidance	1974.64	25.9	1956.51	37.6
		Ours	27.02	25.5	42.55	28.7

6.3. Analysis

Inference costs. We evaluate inference costs in real-world experiments. We generate 1,000 samples and report the average generation time and trajectory length in Table 5. For scalarization, our method takes approximately 10–30 milliseconds longer per sample than MOGFN and HN-GFN, due to the overhead of querying multiple base models. The gap is larger on QM9 partly because our method generates longer trajectories. Despite this overhead, our method offers the flexibility to incorporate new objectives without retraining. For logical operators, our method is approximately 40–70 times faster than classifier-guided mixing, while both methods generate trajectories of similar length except for three objectives on QM9. The reason is that classifier guidance must enumerate and evaluate all successor states at every step to compute the guidance term, whereas our method only requires computation at the current state. Notably, our implementation does not parallelize forward passes of base models. These results demonstrate that our training-free approach incurs minimal inference overhead while eliminating the need for additional training.

Table 6. Validity of generated molecules on the atom-based molecule generation task. We report the percentage of valid molecules among 1,000 generated samples. Note that the base models achieve near-perfect validity (p_{GAP} : 100%, p_{QED} : 99.3%, p_{SA} : 100%).

	Classifier guidance	Ours
$p_{GAP} \otimes p_{SA}$	86.8	99.6
$p_{GAP} \otimes p_{SA} \otimes p_{QED}$	54.8	99.8

Validity of generated molecules. We observe that classifier guidance significantly degrades the validity of generated molecules on QM9, as shown in Table 6. While base models achieve near-perfect validity, the classifier-guided approach drops to 86.8% with two objectives and further degrades to 54.8% with three objectives. We conjecture that classifier guidance may steer the sampling process toward invalid regions of the molecular space. In contrast, our mixing policy maintains validity comparable to the base models, as it directly combines the learned forward policies without introducing external guidance that may conflict with the underlying generative process.

7. Conclusion

In this work, we propose a training-free method for composing pre-trained GFlowNets via a simple mixing rule over learned forward policies. For linear scalarization, we theoretically prove that our mixing rule exactly recovers the target composition distribution. For more general operators, we empirically verify that our method accurately approximates the target distribution in high-density regions most relevant to generation. Experiments on 2D grid and molecule generation tasks demonstrate that our method achieves competitive performance with existing baselines while offering superior efficiency, as it requires no additional training or auxiliary classifiers.

Impact Statement

This paper presents work whose goal is to advance the field of Machine Learning. The primary application of our method is molecular generation for drug discovery, where composing pre-trained GFlowNets can accelerate the exploration of candidates balancing multiple therapeutic properties such as binding affinity, synthetic accessibility, and drug-likeness. By eliminating the need for retraining, our approach reduces computational costs and energy consumption, potentially democratizing access to multi-objective generative modeling for resource-constrained researchers. As with any molecular generation technology, dual-use concerns exist; however, our method composes existing models rather than introducing fundamentally new capabilities, and the generation of candidate molecules remains only one step in a complex pipeline requiring synthesis and experimental validation. We encourage continued development of safety guidelines and best practices for responsible deployment of generative models in scientific discovery.

References

- Bengio, E., Jain, M., Korablyov, M., Precup, D., and Bengio, Y. Flow network based generative models for non-iterative diverse candidate generation. In *Advances in Neural Information Processing Systems*, volume 34, pp. 27381–27394, 2021.
- Bengio, Y., Lahlou, S., Deleu, T., Hu, E. J., Tiwari, M., and Bengio, E. GFlowNet foundations. *Journal of Machine Learning Research*, 24(210):1–55, 2023.
- Bickerton, G. R., Paolini, G. V., Besnard, J., Muresan, S., and Hopkins, A. L. Quantifying the chemical beauty of drugs. *Nature Chemistry*, 4(2):90–98, 2012.
- Chen, Y. and Mauch, L. Order-preserving GFlowNets. In *International Conference on Learning Representations*, 2024.
- Dhariwal, P. and Nichol, A. Diffusion models beat GANs on image synthesis. In *Advances in Neural Information Processing Systems*, volume 34, pp. 8780–8794, 2021.
- Du, Y., Li, S., and Mordatch, I. Compositional visual generation with energy based models. In *Advances in Neural Information Processing Systems*, volume 33, pp. 6637–6647, 2020.
- Du, Y., Li, S., Sharma, Y., Tenenbaum, J. B., and Mordatch, I. Unsupervised learning of compositional energy concepts. In *Advances in Neural Information Processing Systems*, volume 34, pp. 15608–15620, 2021.
- Du, Y., Durkan, C., Strudel, R., Tenenbaum, J. B., Dieleman, S., Fergus, R., Sohl-Dickstein, J., Doucet, A., and Grathwohl, W. Reduce, reuse, recycle: Compositional generation with energy-based diffusion models and MCMC. In *International Conference on Machine Learning*, pp. 8489–8510. PMLR, 2023.
- Ertl, P. and Schuffenhauer, A. Estimation of synthetic accessibility score of drug-like molecules based on molecular complexity and fragment contributions. *Journal of Cheminformatics*, 1(1):8, June 2009. doi: 10.1186/1758-2946-1-8.
- Garipov, T., De Peuter, S., Yang, G., Garg, V., Kaski, S., and Jaakkola, T. Compositional sculpting of iterative generative processes. In *Advances in Neural Information Processing Systems*, volume 36, pp. 12665–12702, 2023.
- Guan, J., Qian, W. W., Peng, X., Su, Y., Peng, J., and Ma, J. 3d equivariant diffusion for target-aware molecule generation and affinity prediction. *arXiv preprint arXiv:2303.03543*, 2023.
- Harris, C., Didi, K., Jamasb, A. R., Joshi, C. K., Mathis, S. V., Lio, P., and Blundell, T. Benchmarking generated poses: How rational is structure-based drug design with generative models? *arXiv preprint arXiv:2308.07413*, 2023.
- Hinton, G. E. Products of experts. In *International Conference on Artificial Neural Networks*, volume 1, pp. 1–6, 1999.
- Hinton, G. E. Training products of experts by minimizing contrastive divergence. *Neural Computation*, 14(8):1771–1800, 2002.
- Ho, J. and Salimans, T. Classifier-free diffusion guidance. In *NeurIPS 2021 Workshop on Deep Generative Models and Downstream Applications*, 2021.
- Huang, Z., Yang, L., Zhou, X., Zhang, Z., Zhang, W., Zheng, X., Chen, J., Wang, Y., Cui, B., and Yang, W. Protein-ligand interaction prior for binding-aware 3d molecule diffusion models. In *The Twelfth International Conference on Learning Representations*, 2024.
- Ingraham, J., Garg, V., Barzilay, R., and Jaakkola, T. Generative models for graph-based protein design. *Advances in neural information processing systems*, 32, 2019.
- Jain, M., Deleu, T., Hartford, J., Liu, C.-H., Hernandez-Garcia, A., and Bengio, Y. GFlowNets for AI-driven scientific discovery. *Digital Discovery*, 2(3):557–577, 2023a.
- Jain, M., Raparthy, S. C., Hernández-García, A., Rector-Brooks, J., Bengio, Y., Miret, S., and Bengio, E. Multi-objective GFlowNets. In *International Conference on Machine Learning*, pp. 14631–14653. PMLR, 2023b.

- Jamil, M. and Yang, X.-S. A literature survey of benchmark functions for global optimization problems. *International Journal of Mathematical Modelling and Numerical Optimisation*, 4(2):150–194, 2013.
- Jang, Y., Kim, D., and Ahn, S. Graph generation with k^2 -trees. In *ICLR*, 2024. URL <https://arxiv.org/abs/2305.19125>.
- Jin, W., Barzilay, R., and Jaakkola, T. Hierarchical generation of molecular graphs using structural motifs. In *International conference on machine learning*, pp. 4839–4848. PMLR, 2020.
- Jo, J., Lee, S., and Hwang, S. J. Score-based generative modeling of graphs via the system of stochastic differential equations. In *International conference on machine learning*, pp. 10362–10383. PMLR, 2022.
- Kingma, D. P. and Ba, J. Adam: A method for stochastic optimization. In *International Conference on Learning Representations*, 2015.
- Koh, H. Y., Zheng, Y., Yang, M., Arora, R., Webb, G. I., Pan, S., Li, L., and Church, G. M. Ai-driven protein design. *Nature Reviews Bioengineering*, 3(12):1034–1056, 2025.
- Landrum, G. RDKit: Open-source cheminformatics. <https://www.rdkit.org/>, 2010. Accessed: 2025-01-05.
- Lee, S., Jo, M., Ok, J., and Kim, D. Enhancing ligand validity and affinity in structure-based drug design with multi-reward optimization. In *International Conference on Machine Learning*, pp. 33129–33142. PMLR, 2025.
- Liao, R., Li, Y., Song, Y., Wang, S., Hamilton, W., Duvenaud, D. K., Urtasun, R., and Zemel, R. Efficient graph generation with graph recurrent attention networks. *Advances in neural information processing systems*, 32, 2019.
- Liu, N., Li, S., Du, Y., Torralba, A., and Tenenbaum, J. B. Compositional visual generation with composable diffusion models. In *European Conference on Computer Vision*, pp. 423–439. Springer, 2022.
- Maas, A. L., Hannun, A. Y., and Ng, A. Y. Rectifier nonlinearities improve neural network acoustic models. In *International Conference on Machine Learning Workshop on Deep Learning for Audio, Speech and Language Processing*, 2013.
- Madan, K., Rector-Brooks, J., Korablyov, M., Bengio, E., Jain, M., Nica, A. C., Bosc, T., Bengio, Y., and Malkin, N. Learning GFlowNets from partial episodes for improved convergence and stability. In *International Conference on Machine Learning*, pp. 23467–23483. PMLR, 2023.
- Malkin, N., Jain, M., Bengio, E., Sun, C., and Bengio, Y. Trajectory balance: Improved credit assignment in GFlowNets. In *Advances in Neural Information Processing Systems*, volume 35, pp. 5955–5967, 2022.
- Martinkus, K., Loukas, A., Perraudin, N., and Wattenhofer, R. Spectre: Spectral conditioning helps to overcome the expressivity limits of one-shot graph generators. In *International Conference on Machine Learning*, pp. 15159–15179. PMLR, 2022.
- Nair, V. and Hinton, G. E. Rectified linear units improve restricted boltzmann machines. In *International Conference on Machine Learning*, pp. 807–814, 2010.
- Nouhi, B., Khodadadi, N., Azizi, M., Talatahari, S., and Gandomi, A. H. Multi-objective material generation algorithm (momga) for optimization purposes. *IEEE Access*, 10:107095–107115, 2022.
- Qu, Y., Qiu, K., Song, Y., Gong, J., Han, J., Zheng, M., Zhou, H., and Ma, W.-Y. Molcraft: structure-based drug design in continuous parameter space. *arXiv preprint arXiv:2404.12141*, 2024.
- Ramé, A., Couairon, G., Shukor, M., Dancette, C., Gaya, J.-B., Soulier, L., and Cord, M. Rewarded soups: Towards Pareto-optimal alignment by interpolating weights fine-tuned on diverse rewards. In *Advances in Neural Information Processing Systems*, volume 36, 2023.
- Ran, N., Wang, Y., and Allmendinger, R. Mollm: Multi-objective large language model for molecular design—optimizing with experts. *arXiv preprint arXiv:2502.12845*, 2025.
- Schulman, J., Levine, S., Abbeel, P., Jordan, M., and Moritz, P. Trust region policy optimization. In *International conference on machine learning*, pp. 1889–1897. PMLR, 2015.
- Schulman, J., Wolski, F., Dhariwal, P., Radford, A., and Klimov, O. Proximal policy optimization algorithms. *arXiv preprint arXiv:1707.06347*, 2017.
- Sutton, R. S., Barto, A. G., et al. *Introduction to reinforcement learning*, volume 135. MIT press Cambridge, 1998.
- Truong Jr, T. and Bepler, T. Poet: A generative model of protein families as sequences-of-sequences. *Advances in Neural Information Processing Systems*, 36:77379–77415, 2023.
- Wortsman, M., Ilharco, G., Gadre, S. Y., Roelofs, R., Gontijo-Lopes, R., Morcos, A. S., Namkoong, H., Farhadi, A., Carmon, Y., Kornblith, S., and Schmidt, L. Model soups: Averaging weights of multiple fine-tuned models improves accuracy without increasing inference

time. In *International Conference on Machine Learning*, pp. 23965–23998. PMLR, 2022.

Yun, S., Jeong, M., Kim, R., Kang, J., and Kim, H. J. Graph transformer networks. In *Advances in Neural Information Processing Systems*, volume 32, pp. 11983–11993, 2019.

Zhang, S., Liu, Y., and Xie, L. Molecular mechanics-driven graph neural network with multiplex graph for molecular structures, 2020. URL <https://arxiv.org/abs/2011.07457>.

Zhou, C., Wang, X., and Zhang, M. Unifying generation and prediction on graphs with latent graph diffusion. *Advances in Neural Information Processing Systems*, 37: 61963–61999, 2024.

Zhu, Y., Wu, J., Hu, C., Yan, J., Hsieh, C.-Y., Hou, T., and Wu, J. Sample-efficient multi-objective molecular optimization with GFlowNets. In *Advances in Neural Information Processing Systems*, volume 36, 2023.

A. Theoretical Details

A.1. Exact Realization for Scalarization

We prove that for scalarization with $\beta = 1$, our mixing rule exactly realizes the target distribution.

Setup. Let $(\mathcal{S}, \mathcal{A})$ be the directed acyclic state graph of a GFlowNet with initial state s_0 , sink state s_f , and terminating states $\mathcal{X} \subset \mathcal{S}$. For each objective $i \in [k]$, we have a pre-trained GFlowNet with forward policy $p_{i,F}(\cdot|s)$, partition function $Z_i > 0$, and terminating state distribution

$$p_i(x) = \frac{R_i(x)}{Z_i}, \quad R_i(x) \geq 0, \quad x \in \mathcal{X}. \quad (10)$$

We write $u_i(s)$ for the reaching probability of s under $p_{i,F}$, satisfying the recursion Eq. (2). Let the scalarization weights be $\omega_i \geq 0$ and define

$$v_i = \frac{\omega_i Z_i}{\sum_{j=1}^k \omega_j Z_j}, \quad \sum_{i=1}^k v_i = 1. \quad (11)$$

Target terminating state distribution. The mixture terminating state distribution satisfies

$$p_M(x) := \sum_{i=1}^k v_i p_i(x) = \frac{\sum_{i=1}^k \omega_i R_i(x)}{\sum_{j=1}^k \omega_j Z_j} \propto \sum_{i=1}^k \omega_i R_i(x). \quad (12)$$

Composed forward policy. Define the mixed reaching probability

$$u_M(s) := \sum_{i=1}^k v_i u_i(s), \quad (13)$$

and the composed forward policy

$$p_{M,F}(s'|s) := \sum_{i=1}^k \frac{v_i u_i(s)}{u_M(s)} p_{i,F}(s'|s) \quad \text{for all } s \in \mathcal{S} \setminus \{s_f\}. \quad (14)$$

Note that Eq. (14) is a special case of the general mixing policy Eq. (4) for scalarization with $\beta = 1$: since \mathcal{G} reduces to a weighted sum, the normalization constant simplifies to $N_M(s) = u_M(s)$.

We now prove that $p_{M,F}$ is a valid policy and induces the desired mixture distribution.

Lemma A.1 (Normalization). For any $s \neq s_f$, $\sum_{s':(s \rightarrow s') \in \mathcal{A}} p_{M,F}(s'|s) = 1$.

Proof. Using Eq. (14) and the fact that each $p_{i,F}(\cdot|s)$ is a probability distribution,

$$\sum_{s'} p_{M,F}(s'|s) = \sum_{i=1}^k \frac{v_i u_i(s)}{u_M(s)} \underbrace{\sum_{s'} p_{i,F}(s'|s)}_{=1} = \frac{\sum_{i=1}^k v_i u_i(s)}{u_M(s)} = 1,$$

where the last equality uses Eq. (13). □

Lemma A.2 (Mixed reaching probabilities). Let u_M be defined by Eq. (13). Then u_M coincides with the reaching probability induced by $p_{M,F}$:

$$\begin{aligned} u_M(s_0) &= 1, \\ u_M(s) &= \sum_{s_*:(s_* \rightarrow s) \in \mathcal{A}} u_M(s_*) p_{M,F}(s|s_*) \quad \forall s \in \mathcal{S} \setminus \{s_0\}. \end{aligned}$$

Proof. The base case $u_M(s_0) = \sum_i v_i u_i(s_0) = \sum_i v_i = 1$ follows from $u_i(s_0) = 1$ and Eq. (11). For $s \neq s_0$, substitute Eq. (14):

$$\begin{aligned} & \sum_{s_*} u_M(s_*) p_{M,F}(s|s_*) \\ &= \sum_{s_*} \left(\sum_{j=1}^k v_j u_j(s_*) \right) \left(\sum_{i=1}^k \frac{v_i u_i(s_*)}{u_M(s_*)} p_{i,F}(s|s_*) \right) \\ &= \sum_{i=1}^k v_i \sum_{s_*} u_i(s_*) p_{i,F}(s|s_*) = \sum_{i=1}^k v_i u_i(s) = u_M(s), \end{aligned}$$

using the reaching probability recursion Eq. (2) in the penultimate equality. \square

Lemma A.3 (State distribution factorization). *For each i , the state probability satisfies*

$$\begin{aligned} p_i(s) &= u_i(s) \rho_i(s) \quad \text{and} \\ p_M(s) &= u_M(s) \rho_M(s), \end{aligned} \tag{15}$$

where $\rho_i(s)$ (resp. $\rho_M(s)$) is the probability of terminating the trajectory when at state s under $p_{i,F}$ (resp. $p_{M,F}$).

Proof. This is the standard GFlowNet factorization: the probability of being at s equals the probability of reaching s times the probability of terminating from s . The equality for p_M follows since $p_{M,F}$ is a valid forward policy by Lemma A.1. \square

Theorem A.4 (Correctness of the composed forward policy). *Let v_i be given by Eq. (11) and $p_{M,F}$ by Eq. (14). Then, for all states s ,*

$$p_M(s) = \sum_{i=1}^k v_i p_i(s). \tag{16}$$

Consequently, the induced terminating state distribution satisfies $p_M(x) = \sum_i v_i p_i(x) \propto \sum_i \omega_i R_i(x)$ for $x \in \mathcal{X}$.

Proof. By Lemma A.3 and the definition of $p_{M,F}$,

$$\begin{aligned} p_M(s) &= u_M(s) \rho_M(s) \\ &= u_M(s) \sum_{i=1}^k \frac{v_i u_i(s)}{u_M(s)} \rho_i(s) \\ &= \sum_{i=1}^k v_i u_i(s) \rho_i(s) \\ &= \sum_{i=1}^k v_i p_i(s), \end{aligned}$$

where the second equality follows from applying Eq. (14) to the termination probability, and the last step uses Eq. (15) for each i . Evaluating Eq. (16) on terminating states $x \in \mathcal{X}$ yields $p_M(x) = \sum_i v_i p_i(x)$; substituting the definitions proves the proportionality claim via Eq. (12). \square

Remarks. (i) The result holds for any non-negative ω_i ; they need not sum to 1. (ii) If estimated partition functions \widehat{Z}_i are used in place of Z_i , the sampler targets the scalarized reward up to a global rescaling, which does not affect the induced distribution. (iii) The support of p_M equals the union of supports of the p_i ; no extra coverage assumptions are required beyond a shared state graph. (iv) This exactness result holds specifically for scalarization with $\beta = 1$. For general composition operators or $\beta \neq 1$, the distortion factor $\delta(x) = u_M(x)/N_M(x)$ introduced in Section 4.2 characterizes the gap between the realized and target distributions.

A.2. Derivation of Reaching Probability Estimator

We derive the reaching probability estimator and discuss how different GFlowNet training objectives affect its availability.

Training objectives and model parameterization. GFlowNet training objectives differ in what quantities they parameterize. Flow Matching (FM) and Detailed Balance (DB) (Bengio et al., 2021) explicitly parameterize the state flow $F(s)$ for all states $s \in \mathcal{S}$, along with the forward policy p_F and backward policy p_B , where the partition function is $Z = F(s_0)$. Sub-Trajectory Balance (SubTB) (Madan et al., 2023) similarly parameterizes the state flow $F(s)$, p_F , and p_B . In contrast, Trajectory Balance (TB) (Malkin et al., 2022) only parameterizes p_F , p_B , and Z , without explicitly learning the state flow $F(s)$. Since our mixing rule requires the reaching probability $u_i(s)$, which can be computed from $F_i(s)$ and Z_i (as we derive below), objectives that explicitly parameterize the state flow (FM, DB, SubTB) are directly compatible with our framework.

Derivation of $u_i(s) = F_i(s)/Z_i$. For any state $s \in \mathcal{S}$, the state flow $F_i(s)$ represents the total flow passing through s :

$$F_i(s) = \sum_{\tau: s \in \tau} F_i(\tau), \quad (17)$$

where the sum is over all complete trajectories τ that pass through s , and $F_i(\tau)$ is the flow along trajectory τ .

Since the total flow equals the partition function, $\sum_{\tau} F_i(\tau) = Z_i$, we can write:

$$\frac{F_i(s)}{Z_i} = \frac{\sum_{\tau: s \in \tau} F_i(\tau)}{\sum_{\tau} F_i(\tau)} = \sum_{\tau: s \in \tau} \frac{F_i(\tau)}{Z_i} = \sum_{\tau: s \in \tau} p_i(\tau), \quad (18)$$

where $p_i(\tau) = F_i(\tau)/Z_i$ is the probability of trajectory τ .

By definition Eq. (1), $u_i(s) = \sum_{\tau \in \mathcal{T}_{s_0, s}} p_i(\tau)$, where $\mathcal{T}_{s_0, s}$ denotes the set of trajectories from s_0 to s . Since the DAG structure ensures that every trajectory starting from s eventually reaches s_f with probability one, this equals $\sum_{\tau: s \in \tau} p_i(\tau)$. Therefore, $u_i(s) = F_i(s)/Z_i$ for all states $s \in \mathcal{S}$.

A.3. Derivation of L_1 Decomposition

We derive the decomposition of the L_1 distance between the induced distribution $p_M(x)$ and the target distribution $p_M^*(x)$ (Eq. (9) in the main text).

Setup. Given k pre-trained GFlowNets with terminating distributions $p_i(x) \propto R_i(x)$, recall from Section 4.2 that the distribution induced by our mixing policy takes the form:

$$p_M(x) = \frac{u_M(x)}{N_M(x)} \cdot \mathcal{G}(p_1(x), \dots, p_k(x)), \quad (19)$$

where $\delta(x) := u_M(x)/N_M(x)$ is the distortion factor.

The target distribution is defined as:

$$p_M^*(x) = \frac{\mathcal{G}(p_1(x), \dots, p_k(x))}{Z_M}, \quad (20)$$

where $Z_M = \sum_x \mathcal{G}(p_1(x), \dots, p_k(x))$ is the partition function.

Derivation. The L_1 distance between the induced and target distributions is:

$$L_1 = \sum_{x \in \mathcal{X}} |p_M(x) - p_M^*(x)|. \quad (21)$$

Substituting the expressions for $p_M(x)$ and $p_M^*(x)$:

$$\begin{aligned} L_1 &= \sum_{x \in \mathcal{X}} |p_M(x) - p_M^*(x)| \\ &= \sum_{x \in \mathcal{X}} \left| \frac{u_M(x)}{N_M(x)} \cdot \mathcal{G}(p_1(x), \dots, p_k(x)) - \frac{1}{Z_M} \cdot \mathcal{G}(p_1(x), \dots, p_k(x)) \right|. \end{aligned} \quad (22)$$

Using the definition of the distortion factor $\delta(x) = u_M(x)/N_M(x)$:

$$L_1 = \sum_{x \in \mathcal{X}} \left| \delta(x) \cdot \mathcal{G}(p_1(x), \dots, p_k(x)) - \frac{1}{Z_M} \cdot \mathcal{G}(p_1(x), \dots, p_k(x)) \right|. \quad (23)$$

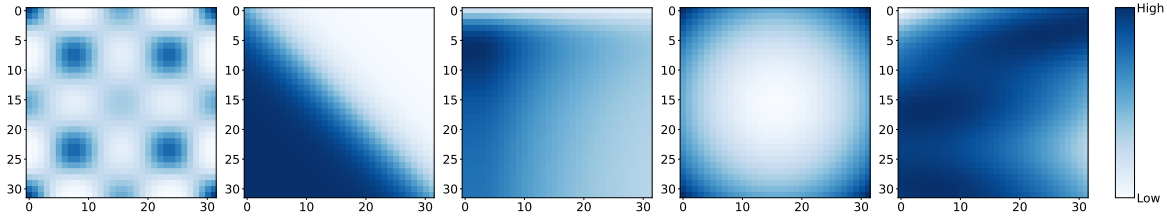
Since $\mathcal{G}(p_1(x), \dots, p_k(x)) \geq 0$ for all x (as it is defined through non-negative reward functions and probability distributions), we can factor it out of the absolute value:

$$L_1 = \sum_{x \in \mathcal{X}} \left| \delta(x) - \frac{1}{Z_M} \right| \cdot \mathcal{G}(p_1(x), \dots, p_k(x)). \quad (24)$$

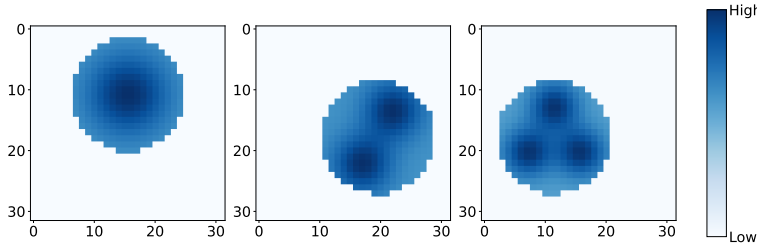
B. Additional Experimental Details

B.1. Synthetic Experiments

Reward functions. We use five reward functions (Figure 1(a)): Shubert, Currin, Sphere, and Branin from multi-objective optimization benchmarks (Jamil & Yang, 2013), and a Diagonal sigmoid reward. All rewards are normalized to $[0, 1]$. We additionally use three synthetic Circle rewards (Figure 1(b)). Each Circle reward defines a Gaussian (mixture) density inside a circular region of radius 0.6 and assigns a constant background reward 0.1 outside the circle.



(a) Five rewards on the 32×32 grid. From left to right: Shubert, Diagonal, Currin, Sphere, and Branin.



(b) Circle rewards on the 32×32 grid. From left to right: Circle1–3.

Figure A1. Visualization of reward functions on the 32×32 grid domain used in our experiments.

Scalarization (Mix- k). We define scalarization targets using weighted-sum rewards over a subset of k objectives. Table A1 lists the objective subsets used in our experiments.

Model details and hyperparameters. All GFlowNets are trained using the Sub-Trajectory Balance (SubTB) (Madan et al., 2023) objective with geometric within-trajectory weighting ($\lambda = 2.0$). Each state is encoded as a 64-dimensional

Table A1. Objective subsets used for Mix- k scalarization (Fig. 1(a)).

	Objectives
Mix2	Shubert, Diagonal
Mix3	Shubert, Diagonal, Currin
Mix4	Shubert, Diagonal, Currin, Sphere
Mix5	Shubert, Diagonal, Currin, Sphere, Branin

K -hot vector (concatenation of two one-hot coordinate vectors). The forward policy p_F and backward policy p_B are MLPs with 2 hidden layers of 64 units and ReLU (Nair & Hinton, 2010) activations, outputting logits over 3 actions (right, down, terminate) and 2 actions (left, up), respectively. The flow estimator F uses the same architecture (2 hidden layers of 64 units) and outputs $\log F(s)$. We train for 20,000 iterations using Adam (Kingma & Ba, 2015) with learning rate 10^{-3} for network parameters and 10^{-1} for $\log Z$, batch size 128, and ϵ -greedy exploration rate 0.05. For base GFlowNets, we additionally use a replay buffer of size 10,000.

For the multi-objective baselines (MOGFN and HN-GFN), preferences are sampled from Dirichlet($\alpha = 1.0$) during training with batch size 128. For MOGFN, state and preference are encoded separately (to 64-dim and 16-dim, respectively) and concatenated before the output head. For HN-GFN (Zhu et al., 2023), each state is first encoded by a fixed MLP encoder with 2 hidden layers of 64 units, and a HyperNetwork with a 3-layer MLP (hidden dimension 32) generates weights for a single linear predictor head.

For the classifier-guided baseline (Garipov et al., 2023), the classifier is an MLP with 2 hidden layers of 64 units and LeakyReLU (Maas et al., 2013) activations. Training uses Adam with learning rate 10^{-3} , batch size 64, and 15,000 iterations. The mixing parameter is sampled as $z \sim \mathcal{U}[-3.5, 3.5]$ with $\alpha = \sigma(z)$. We use an EMA target network (smoothing factor 0.995) and linearly increase the non-terminal loss weight γ from 0 to 1 over the first 3,000 steps.

Additional results. Table A2 and Figs. A2 to A6 show additional results across diverse reward combinations.

Table A2. Extended results of Table 2. L_1 error on logical operators in a 2D grid. We evaluate harmonic mean (\otimes) and contrast (\odot) operations across different reward pairs.

	Classifier guidance	Ensemble	Ours
<i>Harmonic mean (\otimes)</i>			
$p_{\text{Shubert}} \otimes p_{\text{Sphere}}$	0.158	0.145	0.136
$p_{\text{Branin}} \otimes p_{\text{Sphere}}$	0.053	0.121	0.110
$p_{\text{Diagonal}} \otimes p_{\text{Shubert}}$	0.142	0.190	0.180
$p_{\text{Circle1}} \otimes p_{\text{Circle2}}$	0.397	0.453	0.229
$p_{\text{Circle1}} \otimes p_{\text{Circle3}}$	0.266	0.476	0.189
$p_{\text{Circle2}} \otimes p_{\text{Circle3}}$	0.108	0.472	0.301
<i>Contrast (\odot)</i>			
$p_{\text{Shubert}} \odot p_{\text{Sphere}}$	0.175	0.175	0.111
$p_{\text{Sphere}} \odot p_{\text{Shubert}}$	0.190	0.162	0.116
$p_{\text{Branin}} \odot p_{\text{Sphere}}$	0.082	0.116	0.080
$p_{\text{Sphere}} \odot p_{\text{Branin}}$	0.073	0.100	0.102
$p_{\text{Diagonal}} \odot p_{\text{Shubert}}$	0.153	0.190	0.158
$p_{\text{Shubert}} \odot p_{\text{Diagonal}}$	0.150	0.190	0.106
$p_{\text{Circle1}} \odot p_{\text{Circle2}}$	0.245	0.356	0.231
$p_{\text{Circle2}} \odot p_{\text{Circle1}}$	0.241	0.390	0.070
$p_{\text{Circle1}} \odot p_{\text{Circle3}}$	0.122	0.413	0.163
$p_{\text{Circle3}} \odot p_{\text{Circle1}}$	0.138	0.407	0.058
$p_{\text{Circle2}} \odot p_{\text{Circle3}}$	0.098	0.327	0.135
$p_{\text{Circle3}} \odot p_{\text{Circle2}}$	0.093	0.286	0.285

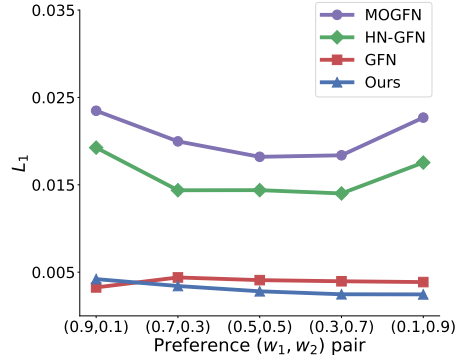


Figure A2. L_1 error for the scalarization of p_{Shubert} and p_{Diagonal} ($\beta = 1$) over five preference vectors $\omega = (w_1, w_2)$. GFN denotes single-objective GFlowNets trained separately for each ω .

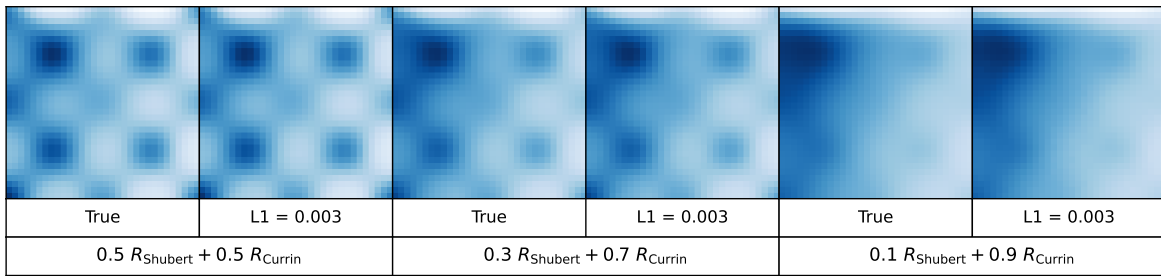


Figure A3. Density visualization of scalarization under different weight settings. For each setting, we show the ground-truth target distribution and the distribution induced by our method, with corresponding L_1 errors.

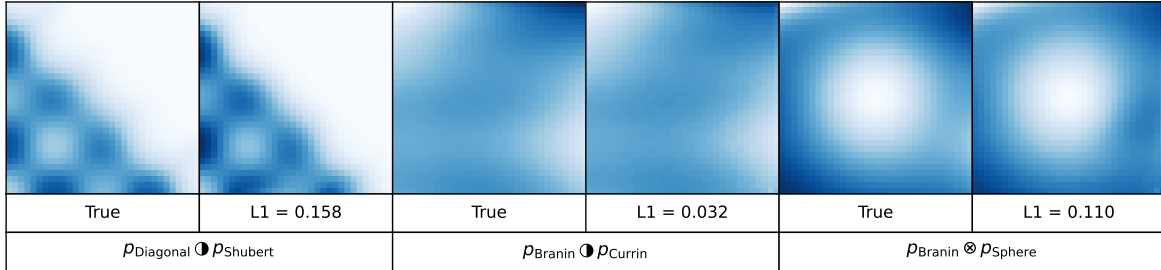


Figure A4. Density visualization of harmonic mean (\otimes) and contrast (\bullet) compositions on pairs of benchmark reward functions. For each composition, we show the ground-truth target distribution and the distribution induced by our method, with corresponding L_1 errors.

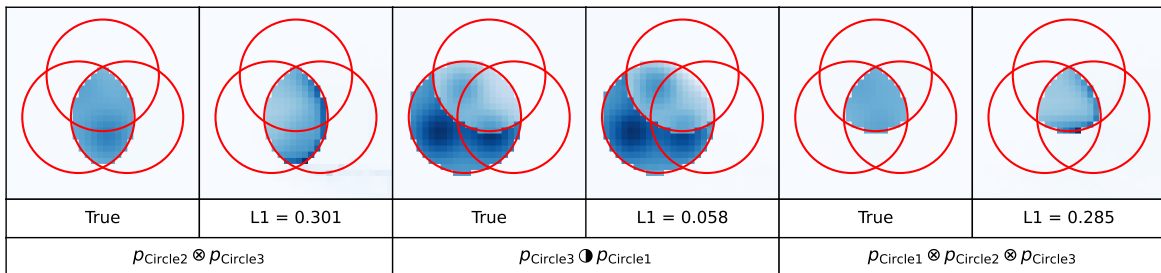


Figure A5. Density visualization of harmonic mean (\otimes) and contrast (\bullet) compositions on Circle rewards. For each composition, we show the ground-truth target distribution and the distribution induced by our method, with corresponding L_1 errors.

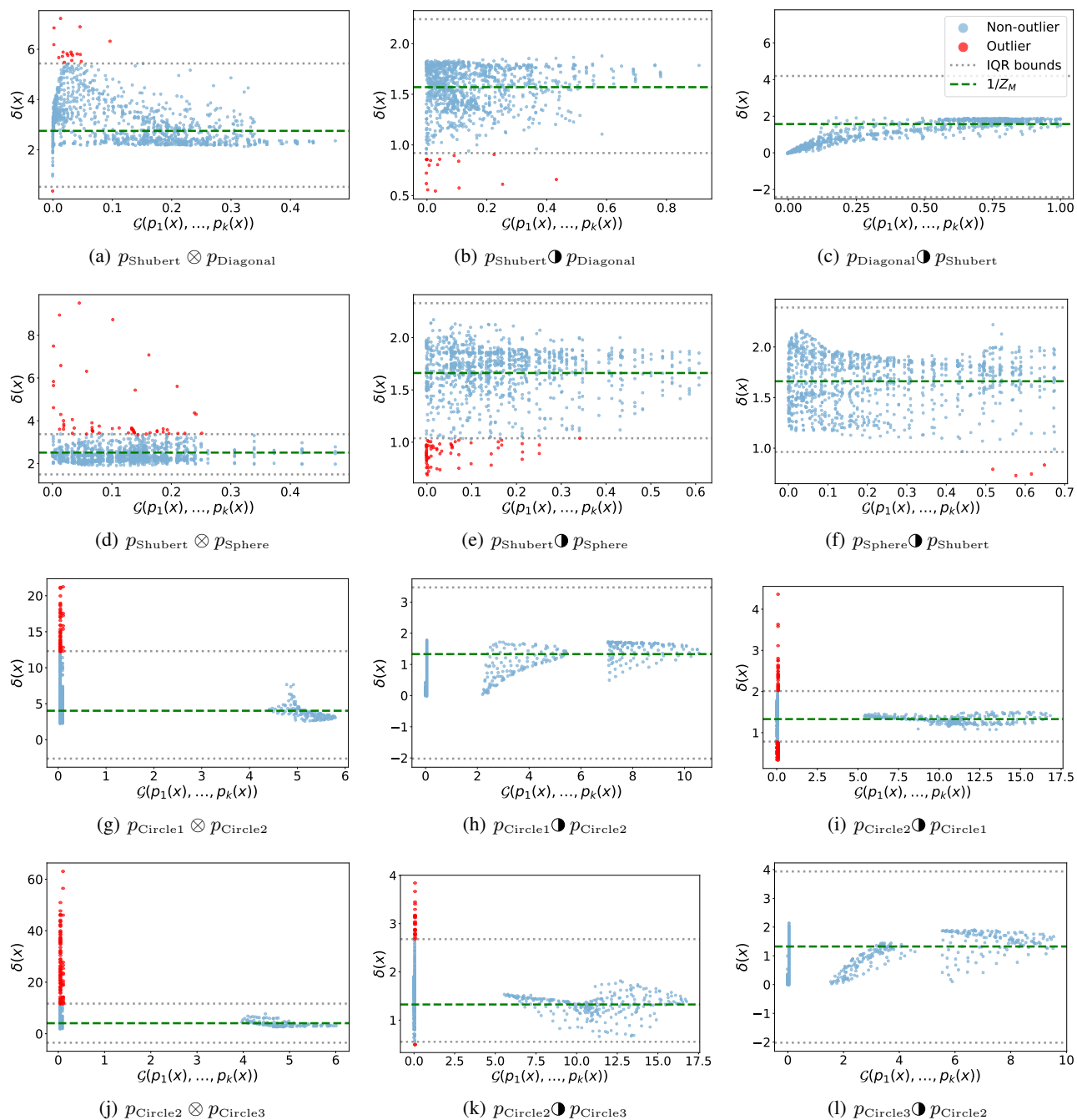


Figure A6. Extended results of Fig. 3. Distortion factor $\delta(x) = u_M(x)/N_M(x)$ vs. unnormalized target density $\mathcal{G}(p_1(x), p_2(x))$ on the 2D grid domain. Red points indicate outliers, defined as states where $\delta(x)$ falls outside $[Q_1 - 1.5 \cdot \text{IQR}, Q_3 + 1.5 \cdot \text{IQR}]$ (gray dotted lines), where Q_1, Q_3 are the 25th/75th percentiles and $\text{IQR} = Q_3 - Q_1$. The green dashed line marks $1/Z_M$ with $Z_M = \sum_x \mathcal{G}(p_1(x), p_2(x))$.

B.2. Real-world Experiments

B.2.1. FRAGMENT-BASED MOLECULE GENERATION

Reward functions. We use three reward functions: **SEH** is the predicted binding affinity to soluble epoxide hydrolase, computed using a pre-trained proxy model (Bengio et al., 2021), with raw values divided by 8 to normalize to approximately $[0, 1]$; **SA** is the synthetic accessibility score (Ertl & Schuffenhauer, 2009), computed using RDKit (Landrum, 2010) and

transformed as $(10 - \text{SA}_{\text{raw}})/9$ to map to $[0, 1]$ with higher values indicating easier synthesis; and **QED** is the quantitative estimate of drug-likeness (Bickerton et al., 2012), computed using RDKit (Landrum, 2010), already in $[0, 1]$.

Model details and hyperparameters. All GFlowNets use a Graph Transformer (Yun et al., 2019) backbone with 6 layers and embedding dimension 128, taking a junction tree representation as input where nodes correspond to fragments and edges encode attachment points. Training uses the Sub-Trajectory Balance (SubTB; (Madan et al., 2023)) objective with Adam (Kingma & Ba, 2015) (learning rate 5×10^{-4} , weight decay 10^{-8}), batch size 64, sampling temperature $\tau = 0.99$, random action probability 0.05, and 15,000 iterations. For single-objective GFlowNets, we use $\beta \in \{32, 64\}$.

For multi-objective baselines (MOGFN and HN-GFN), preferences $\omega \in \Delta^{k-1}$ are sampled from Dirichlet($\alpha = 1.0$) during training, with $\beta = 64$. MOGFN conditions the model by concatenating preferences to the graph-level embedding before the output heads. HN-GFN (Zhu et al., 2023) uses a HyperNetwork with a 3-layer MLP (hidden dimension 100) to generate policy network weights from preferences.

For the classifier-guided baseline, we train a 3-way joint classifier $p(y_1, y_2, y_3 | s)$ following Garipov et al. (2023). The classifier is a Graph Transformer with 4 layers, 2 attention heads, and embedding dimension 128, outputting a $3 \times 3 \times 3$ joint probability tensor. We condition on a terminal indicator and train for 15,000 iterations using Adam (learning rate 10^{-3} , weight decay 10^{-6} , batch size 8 per distribution). An EMA target network (smoothing 0.995) provides stable targets, with non-terminal loss weight γ linearly increasing from 0 to 1 over the first 4,000 steps. Training samples trajectories from pre-trained single-objective GFlowNets (SEH, SA, QED with $\beta = 32$).

Mixing reward-sharpened GFlowNets for scalarization. For the scalarization target $p_M^*(x) \propto (\sum_i w_i R_i(x))^\beta$, we leverage pre-trained ingredient GFlowNets trained on R_i^β . In our mixing framework (Section 4.1), sampling from $p_M^*(x)$ requires ingredient models with terminating distributions $p_i(x) \propto R_i(x)$, which we can then mix as $p_{M,F} \propto (\sum_i w_i Z_i u_i p_{i,F})^\beta$. However, our ingredient GFlowNets are trained with reward exponent β , inducing terminating distributions $\tilde{p}_i(x) \propto R_i(x)^\beta$ with partition functions $\tilde{Z}_i = \sum_x R_i(x)^\beta$.

The unnormalized reward can be recovered as $R_i(x) = (\tilde{Z}_i \tilde{p}_i(x))^{1/\beta}$, since $\tilde{Z}_i \tilde{p}_i(x) = R_i(x)^\beta$. Substituting into the scalarization target:

$$p_M^*(x) \propto \left(\sum_{i=1}^k w_i (\tilde{Z}_i \tilde{p}_i(x))^{1/\beta} \right)^\beta. \quad (25)$$

The mixing policy is therefore:

$$\tilde{p}_{M,F}(s' | s) \propto \left(\sum_{i=1}^k w_i (\tilde{Z}_i \tilde{u}_i(s) \cdot \tilde{p}_{i,F}(s' | s))^{1/\beta} \right)^\beta, \quad (26)$$

which allows composing pre-trained reward-sharpened models without retraining for each preference vector w .

B.2.2. ATOM-BASED MOLECULE GENERATION

Reward functions. We use three reward functions: **GAP** is the HOMO–LUMO gap predicted by an MXMNet (Zhang et al., 2020) proxy trained on QM9, normalized using percentile-based scaling and clipped to $[0, 2]$; **SA** is the synthetic accessibility score (Ertl & Schuffenhauer, 2009), computed using RDKit (Landrum, 2010) and transformed as $(10 - \text{SA}_{\text{raw}})/9$ to map to $[0, 1]$; and **QED** is the quantitative estimate of drug-likeness (Bickerton et al., 2012), computed using RDKit (Landrum, 2010), already in $[0, 1]$.

Model details and hyperparameters. All GFlowNets use a Graph Transformer (Yun et al., 2019) backbone with 4 layers and embedding dimension 64, taking the current molecular graph as input with node features encoding atom types and edge features encoding bond types. Training uses the Sub-Trajectory Balance (SubTB; (Madan et al., 2023)) objective with Adam (Kingma & Ba, 2015) (learning rate 5×10^{-4} , weight decay 10^{-8}), batch size 64, sampling temperature $\tau = 0.99$, random action probability 0.05, and 15,000 iterations. For single-objective GFlowNets, we use $\beta = 32$.

For multi-objective baselines (MOGFN and HN-GFN), preferences $\omega \in \Delta^{k-1}$ are sampled from Dirichlet($\alpha = 1.0$) during training, with $\beta = 32$. MOGFN conditions the model by concatenating preferences to the graph-level embedding before the

output heads. HN-GFN (Zhu et al., 2023) uses a HyperNetwork with a 3-layer MLP (hidden dimension 100) to generate policy network weights from preferences.

For the classifier-guided baseline, we train a 3-way joint classifier $p(y_1, y_2, y_3 | s)$ following Garipov et al. (2023). The classifier is a Graph Transformer with 4 layers, 2 attention heads, and embedding dimension 128, outputting a $3 \times 3 \times 3$ joint probability tensor. We condition on a terminal indicator and train for 15,000 iterations using Adam (learning rate 10^{-3} , weight decay 10^{-6} , batch size 8 per distribution). An EMA target network (smoothing 0.995) provides stable targets, with non-terminal loss weight γ linearly increasing from 0 to 1 over the first 4,000 steps. Training samples trajectories from pre-trained single-objective GFlowNets (GAP, SA, QED with $\beta = 32$).

Mixing reward-sharpened GFlowNets for scalarization. As in the fragment-based setting (Section B.2.1), we leverage pre-trained ingredient GFlowNets trained on R_i^β to sample from the scalarization target $p_M^*(x) \propto (\sum_i w_i R_i(x))^\beta$.

B.2.3. ADDITIONAL RESULTS

Tables A3 to A6 and Fig. A7 show additional results.

Table A3. Results of logical operators with our mixing policy on molecule generation tasks. We report the percentage of samples falling into each of 8 bins based on reward thresholds: Fragment-based (SEH: 0.5, SA: 0.6, QED: 0.25) and Atom-based (GAP: 0.85, SA: 0.4, QED: 0.4). **Bold** indicates the *target bin*: for harmonic mean (\otimes), where all objectives are high; for contrast (\ominus), where only the first objective is high. Classifier-guided results are in Tables A4 and A5.

	Fragment-based									Atom-based (QM9)									
	SEH		low		high		GAP			low		high		SA		low		high	
	SA	low	high	low	high	low	high	SA		low	high	low	high	low	high	low	high		
	QED	low	high	low	high	low	high	low		high	low	high	low	high	low	high			
<i>Base distributions</i>																			
p_{SEH}	0	0	0	0	60	9	28	3	p_{GAP}	1	0	0	0	74	10	13	2		
p_{SA}	0	0	74	6	0	0	17	3	p_{SA}	0	0	10	81	0	0	2	7		
p_{QED}	0	39	0	26	0	22	0	13	p_{QED}	0	4	0	3	12	66	2	13		
<i>Harmonic mean (\otimes)</i>																			
$p_{SEH} \otimes p_{SA}$	1	0	3	1	3	0	81	11	$p_{GAP} \otimes p_{SA}$	0	1	3	4	4	13	23	52		
$p_{SEH} \otimes p_{QED}$	0	5	0	3	0	62	0	30	$p_{GAP} \otimes p_{QED}$	0	0	0	0	30	58	4	8		
$p_{SA} \otimes p_{QED}$	0	5	0	70	0	2	0	23	$p_{SA} \otimes p_{QED}$	0	1	5	53	0	5	3	33		
$p_{SEH} \otimes p_{SA} \otimes p_{QED}$	0	2	0	8	0	15	1	74	$p_{GAP} \otimes p_{SA} \otimes p_{QED}$	0	3	2	11	3	23	8	50		
<i>Contrast (\ominus)</i>																			
$p_{SEH} \ominus p_{SA} \ominus p_{QED}$	1	0	0	0	67	9	21	2	$p_{GAP} \ominus p_{SA}$	0	0	0	0	82	4	13	1		
$p_{SA} \ominus p_{SEH} \ominus p_{QED}$	0	0	83	4	0	0	12	1	$p_{GAP} \ominus p_{QED}$	0	0	0	0	83	4	12	1		
$p_{QED} \ominus p_{SEH} \ominus p_{SA}$	0	45	0	21	0	23	0	10	$p_{GAP} \ominus p_{SA} \ominus p_{QED}$	0	0	0	0	85	3	12	0		

Effect of reward correlations. The effectiveness of the contrast operator depends on the correlation structure of the underlying reward distributions. Table A6 illustrates challenging cases: contrast operations such as $p_{QED} \ominus p_{GAP}$ and $p_{SA} \ominus p_{QED}$ show limited separation. As shown in Fig. A7, we observe that among samples generated by the trained GFlowNets, those with high QED tend to also have high GAP, and those with high SA tend to have high QED. When rewards exhibit such positive correlations in the generated samples, the contrast operator struggles to isolate the target region since samples that score high on one objective inherently tend to score high on the other. In contrast, the compositions reported in Table A3 involve reward pairs with weaker correlations, where the contrast operator successfully isolates the desired regions.

Training-free Composition of Pre-trained GFlowNets for Multi-Objective Generation

Table A4. Results of logical operators with classifier-guided mixing policy on fragment-based molecule generation. We report the percentage of samples falling into each of 8 bins based on reward thresholds: Fragment-based (SEH: 0.5, SA: 0.6, QED: 0.25). **Bold** indicates the *target bin*: for harmonic mean (\otimes), where all objectives are high; for contrast (\ominus), where only the first objective is high.

	SEH		low				high			
	SA		low		high		low		high	
	QED		low	high	low	high	low	high	low	high
(a) p_{SEH}	0	0	0	0	60	9	28	3		
(b) p_{SA}	0	0	74	6	0	0	17	3		
(c) p_{QED}	0	39	0	26	0	22	0	13		
$p_{\text{SEH}} \otimes p_{\text{SA}}$	1	0	14	1	4	2	67	11		
$p_{\text{SEH}} \otimes p_{\text{QED}}$	0	11	0	6	2	52	3	26		
$p_{\text{SA}} \otimes p_{\text{QED}}$	0	7	2	50	0	4	2	35		
$p_{\text{SEH}} \otimes p_{\text{SA}} \otimes p_{\text{QED}}$	1	5	5	18	2	13	14	42		
$p_{\text{SEH}} \ominus p_{\text{SA}} \ominus p_{\text{QED}}$	1	0	1	0	60	7	29	2		
$p_{\text{SA}} \ominus p_{\text{SEH}} \ominus p_{\text{QED}}$	0	0	74	6	0	0	16	4		
$p_{\text{QED}} \ominus p_{\text{SEH}} \ominus p_{\text{SA}}$	0	38	0	24	0	24	0	14		

Table A5. Results of logical operators with classifier-guided mixing policy on atom-based molecule generation (QM9). We report the percentage of samples falling into each of 8 bins based on reward thresholds: Fragment-based (GAP: 0.85, SA: 0.4, QED: 0.4). **Bold** indicates the *target bin*: for harmonic mean (\otimes), where all objectives are high; for contrast (\ominus), where only the first objective is high.

	GAP		low				high			
	SA		low		high		low		high	
	QED		low	high	low	high	low	high	low	high
$p_{\text{GAP}} \otimes p_{\text{SA}}$	3	1	7	6	15	11	24	33		
$p_{\text{GAP}} \otimes p_{\text{QED}}$	1	1	1	0	30	51	6	10		
$p_{\text{SA}} \otimes p_{\text{QED}}$	1	3	5	44	5	10	4	28		
$p_{\text{GAP}} \otimes p_{\text{SA}} \otimes p_{\text{QED}}$	7	1	7	6	28	16	14	21		
$p_{\text{GAP}} \ominus p_{\text{SA}}$	1	0	0	0	74	11	12	2		
$p_{\text{GAP}} \ominus p_{\text{QED}}$	1	0	0	0	74	11	12	2		
$p_{\text{SA}} \ominus p_{\text{GAP}}$	0	0	13	77	0	0	2	8		
$p_{\text{SA}} \ominus p_{\text{QED}}$	0	0	13	77	0	0	2	8		
$p_{\text{QED}} \ominus p_{\text{GAP}}$	1	4	0	2	12	67	2	12		
$p_{\text{QED}} \ominus p_{\text{SA}}$	1	4	0	2	12	67	2	12		
$p_{\text{GAP}} \ominus p_{\text{SA}} \ominus p_{\text{QED}}$	1	0	0	0	74	10	13	2		
$p_{\text{SA}} \ominus p_{\text{GAP}} \ominus p_{\text{QED}}$	0	0	12	78	0	0	2	8		
$p_{\text{QED}} \ominus p_{\text{GAP}} \ominus p_{\text{SA}}$	1	3	0	3	12	66	2	13		

Table A6. Challenging cases of the contrast operator on atom-based molecule generation (QM9). We report the percentage of samples falling into each of 8 bins based on reward thresholds (GAP: 0.85, SA: 0.4, QED: 0.4). **Bold** indicates the *target bin*: for contrast (\ominus), where only the first objective is high.

	GAP		low				high			
	SA		low		high		low		high	
	QED		low	high	low	high	low	high	low	high
p_{GAP}	1	0	0	0	74	10	13	2		
p_{SA}	0	0	10	81	0	0	2	7		
p_{QED}	0	4	0	3	12	66	2	13		
$p_{\text{SA}} \ominus p_{\text{QED}}$	0	0	12	78	0	0	3	7		
$p_{\text{QED}} \ominus p_{\text{GAP}}$	0	4	0	3	8	68	2	15		
$p_{\text{SA}} \ominus p_{\text{GAP}} \ominus p_{\text{QED}}$	0	0	9	85	0	0	1	5		
$p_{\text{QED}} \ominus p_{\text{GAP}} \ominus p_{\text{SA}}$	0	4	0	3	5	73	1	14		

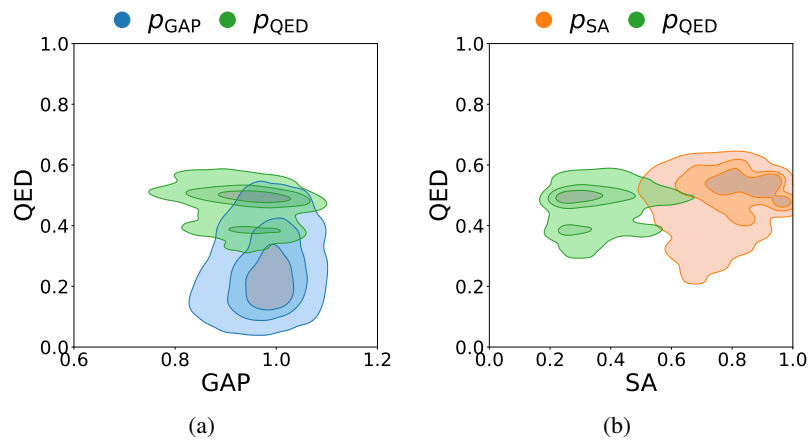


Figure A7. Reward distributions of base models in QM9, illustrating positive correlations between objectives. We observe that (a) High QED samples tend to have high GAP, and (b) High SA samples tend to have high QED.